This is an Accepted Manuscript of an article published by Taylor & Francis in Journal of hydraulic research on 18 August 2020, available online: https://www.tandfonline.com/doi/abs/10.1080/00221686.2020.1780489?journalCode=tjhr20

Hydraulic Resistance in Mixed Bedrock-Alluvial Meandering Channels

ROBERTO FERNÁNDEZ (IAHR Member), PhD Student and Research Assistant, Ven Te Chow Hydrosystems Laboratory, *Department of Civil and Environmental Engineering, University of Illinois at Urbana-Champaign, USA*

Email: fernan25@illinois.edu (author for correspondence)

ALEJANDRO J. VITALE, *Professor, Departamento de Geografía y Turismo, Universidad Nacional del Sur and Researcher, Instituto Argentino de Oceanografía, Consejo Nacional de Investigaciones Científicas y Técnicas (CONICET), Bahía Blanca, Buenos Aires, Argentina.*

Email: vitale.alejandro@gmail.com

GARY PARKER (IAHR Member), Professor, Ven Te Chow Hydrosystems Laboratory, *Department of Civil and Environmental Engineering and W.H. Johnson Professor, Department of Geology, University of Illinois at Urbana-Champaign, USA*

Email: parkerg@illinois.edu

MARCELO H. GARCÍA (IAHR Member), M.T. Geoffrey Yeh Chair and Director, *Ven Te Chow Hydrosystems Laboratory, Department of Civil and Environmental Engineering, University of Illinois at Urbana-Champaign, USA*

Email: mhgarcia@illinois.edu

Running Head: (up to seven words) Hydraulic resistance in bedrock-alluvial meandering channels

Hydraulic Resistance in Mixed Bedrock-Alluvial Meandering Channels

ABSTRACT

We present an experimental analysis of hydraulic roughness variations due to changes in alluvial cover in a mixed bedrock-alluvial meandering channel with larger bedrock roughness than alluvial roughness. Three sets of experiments were conducted in a highly sinuous flume: one with bare bedrock, and two with enough sediment to cover 21% and 78% of the bedrock respectively. We compare our results with data from experiments previously conducted in the same flume with flat- and smooth- bed, and data from experiments with fully alluvial conditions. Our results show that: (i) hydraulic resistance in a mixed bedrock-alluvial channel changes with the degree of alluviation; (ii) hydraulic resistance is greater for bare-bedrock conditions, and decreases as sediment supply increases; (iii) if bedforms appear, hydraulic resistance may be larger than of bare bedrock conditions due to form drag; (iv) fluctuations in alluvial cover due to freely-migrating bars lead to instantaneous changes in hydraulic resistance.

Keywords: Alluvial cover; bars; bed roughness; bedforms; bedload; hydraulic resistance; meandering

1 Introduction

Hydraulic roughness is typically described in terms of a reach-averaged friction factor. In the case of alluvial rivers, this coefficient depends on the size of the material on the bed (skin friction) and, if present, on the size of bedforms (form drag). In the case of mixed bedrock-alluvial rivers (Turowski, 2008), the definition of an appropriate roughness coefficient is more challenging since it also depends on the size of the roughness of the bedrock elements, i.e. the macro-roughness (Zhang et al. 2016), and the percentage of areal cover of alluvium, defined as the ratio of area covered with sediment to total area (e.g. Sklar and Dietrich, 2004).

The role of alluvial cover on hydraulic resistance has been described by a few authors based on experimental measurements (Hodge and Hoey, 2016a, b; Chatanantavet and Parker, 2008; Finnegan et al. 2007), field observations (Ferguson et al., 2017a, b; Hodge et al., 2011), and theoretical considerations complemented with numerical modeling (Johnson, 2014; Inoue et al., 2014; Nelson et al., 2014; Nelson and Seminara, 2012). Of particular interest are the following two scenarios:

i. Alluvial roughness > bedrock roughness: In this condition, the critical shear stress required to mobilize a grain of sediment is greater when it is over alluvium than when it is over bedrock (e.g. Hodge et al. 2016, 2011; Inoue et al., 2014; Chatanantavet and Parker, 2008). Under such conditions, runaway alluviation and throughput bedload are two possible scenarios. The first one may occur when the shear stress drops below the critical value for the bedrock. As soon as sediment starts to deposit, the bed roughness increases drastically leading to runaway alluviation. The second condition might occur when, under a fully alluvial bed, the shear stress rises above the critical value needed to mobilize the alluvium. If patches of bedrock become exposed, the roughness will decrease and therefore sediment will become more mobile until all the bed is depleted of sediment. If sediment continues to be supplied from upstream at the same rate, particles will simply roll, slide, and saltate out of the reach as throughput bedload (Inoue et al., 2014).

ii. Bedrock roughness > alluvial roughness: In this condition, it is harder to move a grain of sediment deposited over bedrock than it is to move a particle lying on a sediment patch (Ferguson et al., 2017a). If sediment continues to be supplied from upstream, it will start filling the holes in the bed until it forms patches. These alluvial deposits will offer less resistance to the flow, and bedload will be preferentially transported over them (Hodge and Hoey, 2016 a, b). If the shear stress increases above the critical shear stress to mobilize grains over the bedrock, the sediment may be washed away rapidly (e.g. Ferguson et al., 2017a, b; Chatanantavet and Parker, 2008).

With the exception of Nelson et al. (2014), all recent work involving alluvial cover in mixed bedrock-alluvial rivers, and its effects on hydraulic resistance, has considered straight- or low-sinuosity reaches. However, channel curvature also increases the resistance to flow, even in the absence of alluvium (e.g. Blanckaert, 2009). We present an experimental analysis of hydraulic roughness in the highly sinuous Kinoshita meandering flume (Abad and Garcia, 2009) at the Ven Te Chow Hydrosystems Laboratory, University of Illinois at Urbana-Champaign (Fig. 1). The main objective of the study is to contribute to a better understanding of hydraulic roughness in mixed bedrock-alluvial meandering rivers where the bedrock roughness is greater than the alluvial roughness.

The study is motivated by the following questions: i) How does the reach-averaged hydraulic roughness in a bedrock river change under different sediment supply scenarios? ii) How do these changes relate to the ratio of areal alluvial cover to total bed area averaged over a reach? iii) How can the composite roughness including the effect of bedrock and alluvium in a channel of complex shape be better described and quantified so as to inform numerical models? iv) How does reach-averaged hydraulic resistance change due to fluctuations in alluvial cover?

In order to answer these questions, we conducted experiments with the three different areal alluvial cover conditions shown in Figure 2. Our analysis also includes data from previous experiments conducted in the same laboratory flume with other bed roughness conditions for comparison. Before proceeding with the description of the experiments, we summarize the relevant definitions used in the analysis.

1.1 Hydraulic resistance

The amount of frictional resistance to which a flow is subjected by a given surface is typically quantified with the use of hydraulic roughness coefficients (Yen, 2002). Common hydraulic roughness coefficients are the Darcy-Weisbach (DW) friction coefficient f, and the dimensionless Chezy friction coefficient C_z.

The shear stress τ_b exerted by a uniform and steady flow on the bed of a channel is given by Eq. 1, where ρ is the fluid density, g is the acceleration of gravity, R_H is the hydraulic radius, S is the slope, and u_* is the shear velocity (Eq. 2). The hydraulic radius is the ratio of the hydraulic area A to the wetted perimeter P. In the case of a rectangular channel, it can be expressed as in Eq. 3, where H is the mean flow depth and B is the channel width.

$$\tau_b = \rho g R_H S = \rho u_*^2 \quad (1)$$

$$u_* = (g R_H S)^{1/2} \quad (2)$$

$$R_H = BH/(B+2H) \quad (3)$$

The average flow velocity U can be determined with the Darcy Weisbach (DW) equation

(Eq. 4). The DW friction coefficient (f) may be related to a general friction coefficient (C_f) as shown in Eq. 5. Both friction coefficients are related to the dimensionless Chezy coefficient (C_z) as shown in Eq. 6.

$$U = (8/f)^{1/2} (gR_HS)^{1/2} = (8/f)^{1/2} u_* \quad (4)$$

$$= f/8 \quad (5)$$

$$C_z = (1/C_f)^{1/2} = (8/f)^{1/2} \quad (6)$$

In this study, the average flow velocity is a known value calculated as shown in Eq. (7) where Q is the flow discharge. An expression for the dimensionless friction coefficient C_f may be obtained by substituting Eq. 5 into Eq. 1 and solving for it as shown in Eq. 8.

$$U = Q/(BH) \quad (7)$$

$$C_f = gR_HS/U^2 = (u_*/U)^2 \quad (8)$$

When the flow is hydraulically rough, the resistance law proposed by Keulegan (1938) may be used to express the bed shear stress, as shown in Eq. 9 where the friction coefficient is given by Eq. 10. Therein, $\kappa = 0.41$ is von Karman's constant, and k_s is the equivalent sand-grain roughness of Nikuradse (1933), which is commonly taken to be proportional to a representative sediment size D_x as shown in Eq. 11. For example, Kamphuis (1974) used $k_s = 2D_{90}$ and Van Rijn (1982) used $k_s = 3D_{90}$, where D_{90} is the size for which 90% of the grains are smaller. Other values commonly adopted for k_s may be found in Garcia (2008).

$$\tau_b = \rho C_f U^2 \quad (9)$$

$$C_f = \{(1/\kappa) \ln[11(R_H/k_s)]\}^{-2} \quad (10)$$

$$k_s = \alpha_s D_x \quad (11)$$

1.2 Alluvial cover

The role of alluvial cover in regard to bedrock incision in mixed bedrock-alluvial rivers was first described by Gilbert (1877), who observed two opposite effects associated with it. Saltating sediment grains are needed for incision by abrasion to occur, i.e. they are the tools required to mechanically wear the bedrock. However, if more and more sediment is added into the system, it will deposit on the bed, thus covering it and protecting it from further incision. The latter phenomenon is typically called the 'cover' effect. Since the work of Sklar and Dietrich (2004), it is usually described in terms of a cover factor p_c, which represents the areal percentage of the bed that is covered with alluvium (Eq. 12).

$$p_c = A_a/A_T = (1 - A_b/A_T) \quad (12)$$

In Eq. 12 A_a is the area covered with alluvium, A_T is the total bed area in the reach, and A_b is the area of exposed bedrock. In the context of this study, an adapted form of Eq. 12 is used to quantify p_c (Eq. 15).

1.3 Partial cover and composite hydraulic resistance

Composite channels are those whose wall roughness changes along the wetted perimeter of the cross section. The need to describe hydraulic resistance using a composite roughness approach has been recognized since, at least, the 1930s. Chow (1959) cites the composite roughness relations due to Horton (1933), Einstein (1934), and Colebatch (1941). Yen (1991) cites a few other relations, namely, Pavlovskii (1931) and Lotter (1933). In general, these relations determine a composite roughness coefficient based on the weighted sum of hydraulic parameters such as the wetted perimeter, hydraulic area, and hydraulic radius.

In the case of mixed bedrock-alluvial channels, Johnson (2014) and Inoue et al. (2014) independently proposed to treat the composite roughness by using a weighted linear summation of the resistance due to alluvial cover and the resistance due to the bedrock surface. Inoue et al. (2014) calculate a total friction coefficient based on a composite equivalent roughness height k_s (Eq. 13). Johnson (2014) first calculates friction coefficients using a Manning-Strickler relation for both the alluvial and bedrock portions of the bed, and then computes a composite friction coefficient as shown in Eq. 14. In both Eqs. 13 and 14, the sub index '*a*' refers to the alluvium and the sub index '*b*' refers to the bedrock.

$$k_s = k_{sa}p_c + k_{sb}(1-p_c) \tag{13}$$

$$f = f_a p_c + f_b(1-p_c) \tag{14}$$

Both approaches are used and compared in this study.

2 Materials and Methods

2.1 Flume

The Kinoshita meandering flume in the Ven Te Chow Hydrosystems Laboratory at the University of Illinois at Urbana-Champaign was used for the experiments presented in this study. The flume, shown in Fig. 1, is 0.60 m wide, 0.40 m deep and 33 m long (along the centerline not including upstream and downstream tanks), and has a sinuosity of 3.7. All three meander wavelengths are identical and are 10 m long as measured along the channel centerline. All results presented herein correspond to experiments conducted with water flowing from right to left as indicated in Fig. 1, i.e. with the bends skewed in the upstream direction. The flume is a closed system with a horizontal bed (no tilting) in which water and sediment are recirculated. Readers interested in more specific details about the Kinoshita flume are referred to the supplemental material and Abad and Garcia (2009).

2.2 Experimental Conditions

We report on a total of ten runs corresponding to four bed roughness conditions. The

conditions first reported herein are: bedrock bed made of concrete with no alluvial cover (Fig. 2a, 3c); mixed bedrock-alluvial with enough sediment to cover 21% of the bedrock bed, as measured over one meander wavelength (Fig. 2b, 3d); and mixed bedrock-alluvial with enough sediment to cover 78% of the bed (Fig. 2c, 3d). Sediment was transported as bed load in both experimental conditions. The case with 78% alluvial cover had freely-migrating bars, whereas no bedforms were present for the case with 21% alluvial cover. The median sediment transport rates measured were 4.65 g/s and 0.07 g/s for the cases of 78% and 21% areal cover respectively. Sediment transport rates were measured by trapping material as it came back to the upstream end of the flume through the recirculating pipe. Several measurements were conducted for a specific amount of time to determine the median transport rate. After collecting the sediment samples, they were dried and weighed.

These measurements are complemented with seven runs conducted in the same flume but with other bed roughness conditions (Fig. 3). Four runs correspond to flat- and hydraulically smooth bed and sediment-free conditions (Fig. 3a), and three to fully alluvial conditions (Fig. 3b). The purpose of including these additional runs is to assess the variations in hydraulic resistance in the same flume with different bed roughness conditions. Table 1 shows the experimental parameters for each of the ten runs. The mean flow depths reported therein correspond to the value measured at the channel centerline at cross section 15 m (Fig. 1a), which is the halfway point of the meandering planform.

2.3 Bed-material properties and bed characteristics

The bed-material used in the experiments with alluvium was crushed walnut shells, which have a specific gravity in the range 1.3-1.4. The purely alluvial bed topography measured by Czapiga (2013) after run A1 (Table 1) was used to build the bedrock bed used in this study. The longitudinal slope of the bed was 1.0×10^{-3} and we calculated the transverse slopes every 0.5 m with the bathymetry. Based on the longitudinal and transverse slopes, foam cross-sections were cut and placed inside the flume. Pea gravel was used to fill the flume following the profile established by the foam. The size of the gravel was chosen so as to prevent it from being transported by the flow in the experiments. The region between streamwise stations CS07 and CS23 (Fig. 1) was filled with gravel to an elevation slightly below the maximum given by the foam. This section was then covered with a ~1 cm thick layer of concrete and used as the bedrock reach. More details about the setup are included in the supplemental material.

The grain size distributions of the crushed walnut shells, the pea gravel, and the dry concrete mix (includes gravel, sand and cement) are shown in Fig. 4. The inset figure includes the results of laser scans conducted to measure the as-built bedrock macro-roughness. A Keyence laser with sub-millimeter precision was used to scan the bed at five different locations, namely: CS10, CS12, CS15, CS17 and CS20 (Fig. 1). A polynomial was

fit to the scans, and residual elevations were calculated by subtracting the actual reading from the polynomial. This removed the effects of topography. The average residual elevation along the cross sections was calculated and used to estimate the macro-roughness of the bedrock bed, defined here as the difference between the maximum and minimum elevations (Zhang et al., 2016). The value thus obtained (10 mm) is also indicated in Fig. 4.

2.4 Water surface elevations

A key and novel aspect of this study is the use of 'eTapes', sensors with a resistive output that varies with the level of fluid (i.e. water). eTapes allow measuring instantaneous water surface elevations, thus making possible the computation of instantaneous water surface slope, which can then be related to hydraulic gradients and resistance.

The three experiments first reported here used eTapes to measure water surface elevations. In the case of the seven experiments conducted previous to these three, water surface elevations were measured with the use of point gages (Czapiga, 2013; Fernández, 2012; Abad and Garcia, 2009).

An eTape is a sensor with a resistive output that varies with the level of fluid in which it is immersed. The resistive output of the sensor is inversely proportional to the height of the water. Low water depths correspond to high output resistance. Conversely, high water depths, correspond to low output resistance.

eTapes were installed inside the flume at the locations shown in Fig. 1a. They were connected to an Arduino Mega board which was programmed to output to a computer terminal at a frequency of 10 Hz. Conversion of the raw sensor output to water levels required calibration. The calibration was conducted to relate the actual water elevation, as read from the marks printed on the sensor, to the electrical output in the computer terminal. The calibration procedure, as well as more details regarding the installation of the eTapes, and a wiring diagram are included in the supplemental material.

For the purpose of our analysis, we compute instantaneous water surface elevation slopes based on the changes in water surface elevation recorded by the eTapes. Before running the experiment, the still water surface elevation was recorded with the eTapes for five minutes. The median value of the readings was then used as the reference level for the values recorded during the run. Water surface elevation changes were calculated relative to this initial value. To obtain the slope, the total change in elevation was divided by the distance between the eTapes (10m).

2.5 Image acquisition

The percentage of areal alluvial cover was calculated by analyzing time-lapse images of the flume. Images were acquired every 10 s (0.1 Hz) with a camera attached to the crane in the

lab and processed in MatLab. A region of interest (ROI) was selected for each image series. In this study, the ROI corresponds to the middle bend of the Kinoshita flume, i.e. between stations CS10 and CS20 (Fig. 1a).

Images were first converted to gray scale and then, the method of Otsu (1979), as implemented in MatLab ('graythresh' function), was used to make the images binary. The resulting black (alluvial cover) and white (bedrock) images were used to calculate the percent areal cover. The fraction of alluvial cover was determined as shown in Eq. 15.

$$p_{cROI} = [N - \sum^{N}_{j=1}(p_{xj})]/N \quad (15)$$

In Eq. 15, p_{cROI} = percent of areal alluvial cover inside the region of interest; N = total number of pixels inside the region of interest (i.e. total area); and p_{xj} = value of the j^{th} pixel in the binary image (white pixels are equal to one and black pixels are equal to zero). More details regarding the image acquisition and processing are included in the supplemental material.

2.6 Hydraulic resistance in the Kinoshita flume

The four kinds of experimental conditions used in this study (Table 1) require different approaches to compute hydraulic resistance. In general, all friction coefficients were calculated with Eq. 8, but due to the different characteristics of the flume setup, the total value thus obtained actually represents a combination of effects.

In the case of the flat bed experiments, hydraulic resistance coefficients are a combination of the resistance due to the walls of the flume and the effect of secondary flow associated with its meandering planform geometry. To quantify these effects, a total Darcy-Weisbach friction coefficient was determined with Eqs. 8 and 6. The Colebrook-White equation for hydraulically smooth flow (Eq. 16) was used to calculate the friction coefficient that would prevail in a straight flume made with the same material as the Kinoshita flume, with a flow with the same Reynolds number R_e (Eq. 17). In Eq. 17, ν is the kinematic viscosity of water.

$$(1/f^{1/2}) = -2\log_{10}[2.51/(R_e f^{1/2})] \quad (16)$$

$$R_e = UR_H/\nu \quad (17)$$

For the four flat- and smooth-bed cases (Table 1), the friction coefficient in Eq. 16 is computed using the solver in Microsoft Excel with the objective function specified in Eq. 18.

$$\{(1/f^{1/2}) + 2\log_{10}[2.51/(R_e f^{1/2})]\}^2 = 0 \quad (18)$$

The difference f_m between these two values, i.e. the Darcy-Weisbach coefficient f, obtained with Eqs. 8 and 6, and the friction coefficient obtained with the Colebrook-White relation

f_{CW} (Eq. 16), is assumed to be due to the meandering geometry of the flume. Eq. 19 shows the total friction coefficient f, as the linear summation of f_{CW} and f_m.

$$f = f_{CW} + f_m \tag{19}$$

The assumption of linearity implied in Eq. 19 has been used extensively in the past (Yen, 1991). For example, Ferguson et al. (2019), Johnson (2014), and Inoue et al. (2014) used it to calculate a composite roughness in mixed bedrock-alluvial channels; Comiti et al. (2009) used it to separate the resistance in step-pool channels in three components: skin, form drag, and spill; Millar (1999) used it to distinguish between skin friction and form drag in gravel bed rivers; and Parker and Peterson (1980) used it to distinguish between skin friction and resistance due to the presence of bars in gravel bed rivers. Many more examples are available in the literature. Yen (1991) presents a review of the historically relevant ones and discusses the issue further. He also includes a section on potential non-linear interactions between the different resistance components. In this study, we continue to use the linear superposition assumption.

In the case of the fully alluvial and mixed bedrock-alluvial experiments, since the bed and the wall have different roughness, the Vanoni and Brooks (1957) wall correction is used to separate the hydraulic resistance between the bed and wall regions. In addition, a shear partition is also required to separate the bed resistance due to skin friction and that due to form drag. The shear partition proposed by Einstein (1950) is used for this purpose. A summary of both methods, as well as their implementation for this analysis is included in the supplemental material. Garcia (2008) also presents a clear description of the Einstein (1950) method.

2.7 Equivalent roughness heights

Eq. 10 may be rewritten in terms of the equivalent roughness height k_s. Eq. 20 shows the result (Garcia, 2008). This equation is used to calculate the equivalent roughness heights for all experimental conditions. The height of the viscous sublayer is computed as shown in Eq. 21. If $k_s > \delta_v$ the flow is hydraulically rough and if $k_s < \delta_v$ the flow is hydraulically smooth.

$$k_s = 11R_H/\exp(\kappa/C_f^{1/2}) \tag{20}$$

$$\delta_v = 11.6\nu/u_* \tag{21}$$

2.8 Quantifying the magnitude of the fluctuations

The instantaneous water surface slopes obtained with the use of the eTape sensors and the quasi-instantaneous areal cover fractions obtained with the time-lapse images are manifested as fluctuating time series. We quantify the magnitude of the fluctuations with the median absolute deviation (MAD) defined in Eq. 22. Therein, X_i corresponds to a single

observation of the sample or population $\boldsymbol{X}$. For example, in the context of this study, $\boldsymbol{X} = \boldsymbol{p_c}$ or $\boldsymbol{X} = \boldsymbol{S_f}$..

$$\text{MAD} = \text{median}[|X_i - \text{median}(X)|] \quad (22)$$

3 Results

3.1 Hydraulic resistance for flat-bed conditions

Table 2 shows the dimensionless friction coefficients (C_f, f, C_z) for the four flat- and smooth-bed experimental conditions (F1-F4 in Table 1). The first column indicates the run ID and the following three columns show the three dimensionless friction coefficients for each run. The 'Total' friction coefficient was calculated with Eq. 8; the 'Wall' friction coefficient was calculated with Eq. 16; and the friction coefficient due to 'Meandering' was calculated with Eq. 19.

The results for the flat bed conditions show that the hydraulic resistance due to meandering in the Kinoshita flume can be a significant component of the total resistance experienced by the flow (Table 2). The resistance coefficient due to meandering f_m (Eq. 19) contributed 6.1%, 56%, 38% and 63% to the total resistance coefficient for runs F1-F4 respectively. This behavior has also been reported by Blanckaert (2009) who compared the hydraulic resistance in a flume between an upstream straight reach and the entire flume, which had a bend of constant curvature. In his results, the overall resistance increased by an average of 40% due to the presence of the bend.

In the cases reported here, smaller values are associated with lower reach-averaged velocities. In the case of runs F2 and F3, the largest contribution obtained for F2 was associated with a larger R_e number, due to larger hydraulic radius in spite of similar reach-averaged velocities.

3.2 Hydraulic resistance for fully alluvial, bare bedrock and mixed bedrock-alluvial conditions

Table 3 shows the dimensionless friction coefficients (C_f, f, C_z) for the fully alluvial (A1-A3), bare bedrock (B1) and mixed bedrock-alluvial (BA1-BA2) experimental conditions. The 'Total' values in the second column were calculated with Eq. 8; the 'Wall' and 'Bed' values in the third and fourth columns were obtained with the Vanoni and Brooks (1957) wall correction; and the resistance in the 'Bed' region was then split into 'Skin' (column 5) and 'Form' drag (column 6) using the shear partition of Einstein (1950). These methods are fully described in the supplemental material.

The redistribution of shear stresses between the wall and bed regions, according to the

Vanoni and Brooks (1957) method, is a weighted average. Therefore, the total friction coefficient does not correspond to the linear summation of the shear stresses in the wall and bed regions. In the case of the Einstein (1950) method, the total shear in the bed region is partitioned between skin and form components. Therefore, the sum of the skin and form friction coefficients (C_f or f) does correspond with the total for the bed region.

To do the shear partitioning for the fully alluvial cases, a value of D_{90} = 1.9 mm was used; for the bare bedrock case, a value of D_{90} = 7.5 mm, based on the grain size distribution of the concrete mix, was used (Fig. 4). In both cases, α_s = 2.5 was used to obtain the equivalent roughness height according to Eq. 11. The shear partition for the mixed bedrock-alluvial runs is not shown in Table 3 because there is no unique particle diameter to represent the roughness height of both surfaces. Instead, the methods of Inoue et al. (2014) (Eq. 13) and Johnson (2014) (Eq.14) were used to estimate composite friction coefficients, due to skin friction for the alluvial and bedrock portions of the bed and the percentage of the bed occupied by alluvium.

In all three alluvial runs, the wall correction of Vanoni and Brooks (1957) reflects an important redistribution of hydraulic resistance due to the increased (beyond the case of a smooth bed) roughness of the bed relative to the walls. The average bed shear was approximately 7 times larger than the wall shear in runs A1 and A2 ($f_{bed}/f_{wall} \sim 7$) and approximately 15.5 times larger in run A3 (Table 3, Fig. 5a). The resistance in the bed region was also split into skin friction and form drag (Einstein, 1950). Skin friction was responsible for 34% - 39% of the hydraulic resistance in runs A1 and A2 respectively, i.e. $f_{skin}/f_{bed} \sim$ 34% - 39%. In run A3, it accounted for 18% of the resistance.

Form drag accounted for 66%, 61% and 82% of the resistance in runs A1-A3 respectively. These percentages include more than just bedforms. Parker and Peterson (1980) attributed part of the resistance they observed to the presence of bars. The results from the flat- and smooth-bed experimental runs show that a significant contribution of the resistance comes from the meandering planform geometry and the associated ubiquitous secondary flows. Even though the fully alluvial runs had bedforms in them (Czapiga, 2013), the form drag is actually a combination of effects: meandering (secondary flows), point bars, and bedforms. The first two are interrelated because point bar geometry is a consequence of the meandering planform characteristics (e.g. Johannesson and Parker, 1989; Ikeda et al., 1981).

The hydraulic resistance within the bed region in the bare bedrock (B1) experiment (Fig. 2a) was almost 6 times larger than that of the wall region (Table 3, Fig. 5a). In this case, skin friction accounted for 60% of the total resistance in the bed region, and form drag for 40%. Even though this run did not have migrating bedforms, the bathymetry resembled that of run A1. Therefore, the form drag was due to both the meandering planform and the bed topography.

The dimensionless friction coefficients (C_f, f, C_z) for the mixed bedrock-alluvial experimental conditions were calculated with the approaches of Inoue et al. (2014) and Johnson (2014). Table 4 shows the results. The first column indicates Run ID and the average ratio of alluvial cover for the middle bend of the Kinoshita flume (Figs. 1, 2b and 2c) in each run. Values for 'Skin' friction and 'Form' drag are included for each run (column 2). Columns 3-5 are related to Eq. 14, i.e. the approach of Johnson (2014) who calculates a friction factor for fully 'Alluvial' conditions (column 3), a friction factor for bare 'Bedrock' conditions (column 4) and then calculates a 'Combined' friction factor (column 5). Column 6 contains the results obtained with the approach of Inoue et al. (2014). A composite equivalent roughness height k_s was calculated with Eq. 13 and then used to split the shear in the bed region between skin friction and form drag.

Figure 5a shows a column-plot of the dimensionless friction coefficients C_f for all runs. Figure 5b shows a comparison between the skin and form friction coefficients obtained with the approaches of Inoue et al. (2014) (Eq. 13) and Johnson (2014) (Eq. 14).

The hydraulic resistance in the bed region was 5 times larger than that in the wall region for run BA1, and 10 times larger for run BA2 (Table 3, Fig. 5a). Both experiments had very similar hydraulic conditions (Table 1) and the main difference between them was the presence of more alluvium in BA2, which contributed to the formation of freely-migrating bars.

The differences between the approaches of Johnson (2014) and Inoue et al. (2014) are smaller than 5% in all cases (Fig. 5b). Specifically, the skin friction between the two approaches differs by approximately 1.9% and 4.2% and the form friction differs by approximately 3.6% and 1.3% for runs BA1 and BA2 respectively. Recently, Ferguson et al. (2019) also obtained similar results with both approaches for data from the Liwu (Taiwan) and Fraser (Canada) rivers and Trout Beck (United Kingdom).

In general, skin friction accounted for 64% of the resistance in the bed region in run BA1 and 28% in run BA2. In the case of BA1, 36% of the total resistance in the bed region corresponds to form drag even in the absence of freely-migrating bedforms (Fig. 5a). As in the bare bedrock (B1) experimental conditions, the form drag is due to the meandering planform and bed topography.

3.3 Hydraulic resistance for mixed bedrock-alluvial experimental conditions with fluctuating alluvial cover due to freely-migrating bars

The previous two sections present results for spatiotemporal averages of hydraulic resistance. However, during experimental Run BA2, freely-migrating bars not only contributed to form drag as shown in Table 4, but also contributed to changes in the ratio of areal alluvial cover. Such changes affect the hydraulic resistance experienced by the flow.

This section presents the fluctuations in hydraulic resistance due to fluctuations in alluvial cover. Simultaneous measurements of water surface elevation and alluvial cover were conducted for 45 minutes in Run BA1 and for 60 minutes in Run BA2. The video included with the supplemental material shows the freely-migrating bars in experiment BA2.

Figure 6 shows temporal series of alluvial cover (Figs. 6a and 6b) and water surface slopes (Figs. 6c and 6d) for Runs BA1 and BA2. The "Instantaneous" series correspond to alluvial cover measured every 10 seconds (Figs. 6a, 6b), and to water surface slope averages computed every 10 seconds (Figs. 6c, 6d). eTape measurements were taken at a frequency of 10 Hz, i.e. one value every 0.1 s, but in order to match the alluvial cover information, window averaging was used for the water surface slopes.

The fluctuations, characterized by the median absolute deviations (Eq. 22) for the alluvial cover in runs BA1 and BA2 are 0.05% and 0.72% respectively. The median absolute deviations for the water surface slopes in runs BA1 and BA2 are 1.8% and 5.7% respectively. Even though the series is not shown, the median absolute deviation for the slopes calculated with the water surface elevations measured during 60 minutes in run B1 is 1.4%. This value may be taken as the baseline for the magnitude of the fluctuations in the eTape signal in the mixed bedrock-alluvial runs. Subtracting it from the values obtained in runs BA1 and BA2 yields deviations of 0.4% and 4.3% respectively. Therefore, the median absolute deviation for alluvial cover in run BA2 was approximately 14 times greater than in run BA1 (0.72%/0.05%) and for the slopes it was approximately 11 times greater (4.3%/0.4%).

The fluctuations in alluvial cover modify the resistance experienced by the flow. Fig. 7 shows the temporal series of the dimensionless friction coefficients for runs BA1 and BA2. The solid black lines correspond to the total friction coefficient in the bed region C_{fb} obtained after applying the wall correction (Vanoni and Brooks, 1957); the dark and light blue lines correspond to the friction coefficient due to form drag C_{ff}; and the dark and light gray lines correspond to the skin friction coefficient C_{fs}. The latter two coefficients were obtained after applying the shear partition of Einstein (1950). The light blue and light gray series were calculated with the approach of Johnson (2014), whereas the dark blue and dark gray series were calculated with the approach of Inoue et al. (2014). The fluctuations in the friction coefficient due to form drag in run BA2 are a consequence of the freely-migrating bars.

3.4 Equivalent roughness heights

Table 5 and Figure 8 show the equivalent roughness height and the thickness of the viscous sublayer for the different runs. The results for the flat bed conditions do not contain values for the wall correction because it was not needed. The 'Meandering' values were used as 'Form' for the computations. Note that due to the form of Eq. 20, the equivalent roughness

heights due to skin and form friction do not add up to the roughness height of the bed region, as is the case with the friction coefficients.

When back-calculated from a Manning's n or Chezy friction coefficient, it is common to find equivalent roughness heights which are larger than the flow depth (Ferguson et al., 2019; Rennie et al., 2018; Garcia, 2008). Given the results shown in Table 5 and Fig. 8, it is not surprising that this is the case if, for instance, the equivalent roughness height relates to a bulk ('total') friction coefficient that is not split into skin and form friction components. Compound equivalent roughness heights k_c have been used in the context of flows with bedforms (e.g. Nelson and Smith, 1989; Wright and Parker, 2004) and they account for both skin friction and form drag. The use of the term 'compound' in this section requires clarification. The term 'composite' is also used in the literature to refer to the equivalent roughness height due to the combined effects of skin friction and form drag. In this paper however, we call it compound roughness to differentiate it from the composite roughness in mixed bedrock-alluvial rivers.

The equivalent, composite and compound roughness heights were calculated with the use of Eq. 20. In general, the roughness heights obtained for the wall regions of the flow are rather small; their values are less than 0.3 mm and 2-3 orders of magnitude smaller than those of the bed region (Fig. 8). For comparison, the height of the viscous sublayer, $\delta_v = 11.6\nu u_*^{-1}$, varies between 0.67 mm (Run A2) and 1.48 mm (Run F1). Since $k_s < \delta_v$ the walls of the Kinoshita flume are hydraulically smooth.

The average bed form heights for runs A1, A3 and BA2 were: 0.05 m, 0.025 m and 0.07 m which correspond to approximately 60% of the centerline flow depth. The roughness heights for the bed region in these runs are larger than the flow depth. This is likely due to the fact that the overall resistance in the bed region also includes form drag due to the meandering planform geometry of the flume.

The equivalent roughness heights in B1 are larger than in BA1 (Fig. 8). This suggests that adding some alluvial cover decreased the overall resistance in the flume, relative to the value prevailing for a pure bedrock bed. This is also shown in Tables 3 and 4 and discussed further in Section 4.1 below. The roughness height of the bed region in run BA2 is 2-3 times larger than in runs B1 and BA1 and in contrast with the latter two, where the skin friction was larger than form drag, the equivalent roughness height associated with form friction in run BA2 is approximately 10 times larger than that due to skin friction. The magnitude of this redistribution in hydraulic resistance due to the presence of bedforms is not captured with the use of Eqs. 13 or 14. Both Johnson (2014) and Inoue et al. (2014) acknowledge this. We discuss the issue further in section 4.2.

4 Discussion

Proper quantification of hydraulic resistance, and associated friction coefficients, continues to be a challenge due to the multiple factors that contribute to it. In the original work of

Nikuradse (1933), resistance was a simple concept associated with a single parameter: sand diameter. In the context of open channel flow, however, hydraulic resistance has many possible sources. Distinguishing each specific contribution is no easy task.

Our results suggest that the fluctuations of alluvial cover in space and time in mixed bedrock-alluvial channels are responsible for quasi-instantaneous changes in hydraulic resistance even under constant flow discharge conditions.

4.1 Experimental conditions

The results for the bedrock and mixed bedrock-alluvial conditions presented in this study are based on instantaneous water surface elevation data measured with two eTapes located on the outside wall of the channel at cross sections 10 m and 20 m (Fig. 1a). The location of the eTapes was chosen for the following reasons: i) the region of interest used to quantify the areal alluvial cover values was defined between cross sections 10 m and 20 m; ii) the eTapes must be attached to a rigid object because they are flat, flexible, and positively buoyant; iii) the eTapes require at least 0.03 m of hydraulic head (submergence) to measure changes in water surface elevation, and these values were only possible at the outer part of the bend due to flow depth and point bar elevation on the inside of the bend.

Due to the meandering planform of the flume, the water surface elevation at the wall is likely to be higher than the water surface elevation at the channel centerline. In spite of this cross-sectional difference in elevation between centerline and outside wall, the longitudinal (reach-length) change in elevation measured at the wall was assumed to be the same as the one at the channel centerline.

An additional aspect related to the meandering planform of the flume is the fact that the flow is not uniform (channel is not straight and prismatic). In spite of this, our analysis of hydraulic resistance assumes uniform flow. Strictly speaking, all flows in natural channels are not uniform. Nevertheless, the assumption of reach-averaged uniform conditions is commonly used to determine resistance coefficients (e.g. Ferguson et al., 2019; Yen, 1992).

4.2 Role of alluvial cover on hydraulic resistance

Our experiments with bedrock and mixed bedrock-alluvial conditions correspond with the case of bedrock roughness greater than alluvial roughness, as discussed in the introduction. The crushed walnut shells are all smaller than 2 mm (D_{90} = 1.9 mm) and the measured bedrock macro-roughness (Zhang et al., 2016) was 10 mm (Fig. 4). Under such conditions, when sediment grains begin to deposit and form an alluvial patch, hydraulic resistance decreases. We observed this between experimental conditions B1 ($p_c = 0$) and BA1 (p_c = 0.21). Smaller friction coefficients were obtained for the case with 21% alluvial cover.

The regions with alluvial cover offer a path of least resistance for sediment grains as they are transported downstream as bedload. It is less likely for a sediment particle to be trapped within the bedrock macro-roughness if it travels over alluvium. We observed this in experiment BA1. Independent sediment grains were transported over the alluvial patches for the most part. Fig. 2b shows two discontinuities in the alluvial cover patches where this was not the case.

The discontinuities correspond to the regions of the bend with the highest curvature, i.e. the two apices. At these locations, between CS14-CS15 and CS19-CS20 (Fig. 1), the sediment particles were transported over the bedrock with the help of the secondary flow. Individual grains were mobilized from the deeper outside area of the bend to the shallower inside area of the bend. Even though we did not measure velocities, our observations suggest that the alluvial patch discontinuities are located at regions of topographically induced high flow velocities, in accordance with observations made by Hodge and Hoey (2016b).

4.3 A third scenario: Alluvial bedform roughness > bedrock roughness

The two possible scenarios discussed in the introduction are specific to skin or grain friction. Experiments B1 and BA1 can be analyzed under that framework. Nevertheless, experiment BA2 suggests there is a third scenario: alluvial bedform roughness > bedrock roughness. This is no surprise and both Johnson (2014) and Inoue et al. (2014) mention it.

In this third scenario, it does not matter if the skin roughness of the alluvium is greater or smaller than that of the bedrock. The presence of freely-migrating bars in experiment BA2 resulted in higher friction coefficients than those in experiment B1, with bare bedrock conditions and therefore, available methods to model morphodynamic evolution of mixed bedrock-alluvial channels must have a limited scope.

The approaches corresponding to Eqs. 13 and 14 do not account for bedforms. However, bedforms can change the friction coefficient up to a factor of five (Garcia, 2008), and therefore, flow depths can increase concomitantly. Accounting for bedforms is important in order to properly quantify the interactions between alluvial cover, transport rates and incision rates in mixed bedrock alluvial rivers.

We propose to modify Eq. 14 so as to incorporate the effect of form drag. For example, a relation like Eq. 23 could be used, where f_{as} is the friction coefficient for alluvial cover due to skin friction and f_{af} is the friction coefficient due to form drag caused by bedforms. Alternatively, using an approach similar to Eq. 13, we propose the use of an equivalent roughness height k_c, that accounts for both the skin friction k_{sa} and form drag k_{sf} as shown in Eq. 24. There are several methods in the literature that use such a compound roughness height (e.g. Wright and Parker, 2004; Nelson and Smith, 1989; Kikkawa and Ishikawa, 1979). Depending on channel scale and context (laboratory or field), and flow regime, one

or another might be better suited to estimate k_c, i.e. the combination of k_{sa} and k_{sf}.

$$f = (f_{as} + f_{af})p_c + f_b(1-p_c) \quad (23)$$

$$k_s = (k_{sa} + k_{sf})p_c + k_b(1-p_c) \quad (24)$$

4.4 *Reach-averaged vs. local hydraulic resistance*

Figure 6a shows that the fluctuations in alluvial cover for run BA2, averaged over one wavelength, vary between 0.75 and 0.80. However, locally, the fluctuations in alluvial cover are much larger. Figure 9 shows a region of the flume close to CS13 (Fig. 1a) at two different times during the run. The local alluvial cover within that window shows values of 0.97 (Fig 9a) and 0.70 (Fig. 9b). These values only represent two instants but are enough to suggest that locally, alluvial cover fluctuations are larger than the values obtained after averaging over one wavelength. The magnitude of the fluctuations will be dependent on the spatial window size used to compute the alluvial cover. Yen (1992) argues that the hydraulic resistance in open channel flows at a point is different than the cross-sectional value and that both are different to the reach-averaged.

The setup used in these experiments does not allow for local calculations of water surface slope fluctuations; thus the local friction coefficients cannot be estimated. Nevertheless, the available measurements at the 'reach' scale (one wavelength) confirm that local fluctuations in alluvial cover have an effect on overall shear stress distribution and, as a consequence, can be expected to affect sediment transport and morphodynamics (Hodge et al., 2016; Inoue et al., 2014; Johnson, 2014; Nelson and Seminara, 2012).

A study of the changes in hydraulic resistance due to local variations in alluvial cover would require similar experiments but, with a denser network of eTapes. Experiments in a straight flume with three or four sets of eTapes on both sides would allow for a better assessment of the changes in local water surface slopes due to local changes in alluvial cover. Instead of conducting experiments with a continuous supply of sediment, it would also be of value to start with bare bedrock, then add sediment into the system for a specific amount of time, and then stopping. The resulting temporal series of alluvial cover and slopes would allow for better quantification of the hydraulic resistance due to the presence of a migrating sediment wave.

A set of such experiments with alluvial roughness smaller and larger than- and similar to-bedrock roughness would also provide a good baseline to determine the sensitivity of the chosen hydraulic roughness heights for the computations of friction coefficients. In our analysis, since the bedrock macro-roughness (10 mm) was five times the size of the largest sediment grain (2 mm), the equivalent roughness heights determined using Eq. 11 and subsequent trends in friction coefficients are not expected to change even if a different value for alpha would have been used.

4.5 Wall correction and narrow bedrock channels

One of the assumptions of the Vanoni and Brooks (1957) procedure for side-wall correction is that the roughness of the bed and wall regions, although different, must be homogeneous within each region. This assumption does not hold in the case of mixed bedrock-alluvial channels because the bed roughness is not homogenous. This procedure should be revisited to incorporate the possibility of more than just two regions. The relevance of the issue is not constrained to laboratory applications.

Many mixed bedrock-alluvial rivers have cross-sections that cannot be assumed to be wide (e.g. Ferguson et al., 2019; Venditti et al., 2014). Moreover, the method should be able to account for the case where the walls are hydraulically rougher than the bed as well (Ferguson et al., 2019). The analyses of Cox (1973) and Yasin (1953) and the experimental programs described therein might prove as a useful starting point to revisit the latter issue in the laboratory.

5 Conclusions

The results presented in this study contribute to a better understanding of hydraulic resistance in mixed bedrock-alluvial channels, and highlight the shortcomings of available methods. Specifically:

1. Hydraulic resistance in a mixed bedrock-alluvial river reach changes with the degree of alluviation.

2. If the bedrock roughness is larger than the alluvial roughness, hydraulic resistance is greater for bare-bedrock conditions, and decreases as sediment supply increases. Insofar the amount of sediment and hydraulic conditions do not lead to the formation of bedforms, the hydraulic resistance is expected to continue to decrease even as sediment supply increases. If bedforms appear, a third scenario in which alluvial bedform roughness exceeds bedrock roughness is possible.

3. Alluvial cover fluctuations change the hydraulic resistance of the flow. With the use of the eTapes we were able to measure this in a quasi-instantaneous manner. Our experimental results suggest that the theoretical approaches of Inoue et al. (2014) and Johnson (2014) yield comparable composite roughness values in mixed bedrock-alluvial channels. The variation between the results obtained with both approaches was smaller than 5%. It is likely that both approaches are equally appropriate to estimate composite roughness in mixed bedrock-alluvial channels.

4. Better quantification of the hydraulic resistance in mixed bedrock-alluvial channels can be achieved by taking into consideration the additional roughness created by the presence of bedforms. The approaches of Inoue et al. (2014) and Johnson (2014) may

be extended to include the effect of bedforms, as we propose in Eqs. 23 and 24. More research is required to assess their applicability.

5. The wall correction of Vanoni and Brooks (1957) must be revisited to better quantify the redistribution of shear between the bed and walls of the channel in mixed bedrock-alluvial rivers. Many such rivers are narrow, and its applicability is therefore not constrained to a laboratory setting.

Acknowledgements

The authors would like to thank Jaclyn Daum for help offered during the installation and first calibration of the instantaneous water surface elevation measuring devices (eTapes). We would also like to thank the associate editor and three anonymous reviewers whose comments to the original draft contributed to improve the manuscript.

Funding

Funding for R. Fernandez and G. Parker was provided by the US National Science Foundation [grant EAR1124482]; A. Vitale was supported by The National Scientific and Technical Research Council of Argentina (Spanish: Consejo Nacional de Investigaciones Científicas y Técnicas, CONICET) and the National Agency for Scientific and Technological Promotion (Spanish: Agencia Nacional de Promoción Científica y Tecnológica); and M.H. Garcia was supported by the M.T. Geoffrey Yeh Endowed Chair in Civil Engineering and a grant from the Illinois Water Resources Center (IWRC). All the support is gratefully acknowledged.

Supplemental data

S1. Description of eTape sensors, wiring diagram, flume installation and calibration, and code to acquire data.

S2. Description of image acquisition for alluvial cover.

S3. Video of experiment BA2 showing freely-migrating bars.

S4. Details about the Vanoni and Brooks (1957) wall correction, and the Einstein (1950) shear partition.

S5. Details about the experimental set up.

Notation

A – hydraulic area (m²)

A_a – area covered with alluvium (m^2)

A_b – area of exposed bedrock (m²)

A_T – total bed area in the reach (m^2)

B – channel width (m)

C_f – dimensionless friction coefficient (-)

C_{fb} – dimensionless friction coefficient in the bed region (-)

C_{fs} – dimensionless friction coefficient due to skin or grain friction (-)

C_{ff} – dimensionless friction coefficient due to form drag (-)

C_z – dimensionless Chezy friction coefficient (-)

D_{90} – grain size for which 90% of the distribution is smaller (m)

D_x – representative sediment size (m)

f – Darcy-Weisbach friction coefficient (-)

f_a – Darcy-Weisbach friction coefficient of the alluvium (-)

f_{as} – friction coefficient due to skin friction of the alluvium (-)

f_{af} – friction coefficient due to form drag of the alluvium (-)

f_b – Darcy-Weisbach friction coefficient of the bedrock (-)

f_{bed} – friction coefficient in the bed region (-)

f_{skin} - friction coefficient due to skin or grain friction (-)

f_{wall} – friction coefficient in the wall region (-)

f_{CW} – friction coefficient calculated with the Colebrook-White equation (-)

f_m – friction coefficient due to meandering (-)

g – gravity constant (ms^{-2})

H – channel depth (m)

k_c – compound roughness height due to skin friction and form drag (m)

k_s – equivalent sand-grain roughness or composite roughness height (m)

k_{sa} – equivalent roughness height of the alluvium due to skin friction (m)

k_{sb} – equivalent roughness height of the bedrock (m)

k_{sf} – equivalent roughness height of the alluvium due to form darg (m)

MAD – median absolute deviation of a variable X

n – Manning's roughness coefficient (-)

N – total numer of pixels inside the ROI

P – wetted perimeter (m)

p_c – areal fraction of alluvial cover, cover factor (-)

$p_{c_{ROI}}$ – percent of areal alluvial cover inside a region of interest (ROI) (-)

p_{xj} – value of the j^{th} pixel in the binary image (-)

Q – flow discharge (m^3s^{-1})

R_e – Reynolds number (-)

R_H – hydraulic radius (m)

ROI – region of interest (in a image) (-)

S – slope (-)

S_f – water surface (friction) slope (-)

u_* – shear velocity (ms^{-1})

U – reach-averaged velocity (ms^{-1})

X – sample or population of any variable

X_i – single observation of X

α_s – dimensionless constant of proportionality between k_s and D_x (-)

δ_v – thickness of the viscous sublayer (m)

κ – von Karman constant (-)

ρ – water density (kgm^{-3})

τ_b – bed shear stress (Pa)

ν – kinematic viscosity of water (m^2s^{-1})

References

Abad, J.D., and Garcia, M.H. (2009) Experiments in a high-amplitude Kinoshita meandering channel: 1. Implications of bend orientation on mean and turbulent flow structure. Water Resources Research, 45, W02401, doi:10.1029/2008WR007016.

Blanckaert, K. (2009) Saturation of curvature-induced secondary flow, energy losses, and turbulence in sharp open-channel bends: Laboratory experiments, analysis, and modeling. Journal of Geophysical Research, 114, F03015, doi: 10.1029/2008JF001137.

Chatanantavet, P., and Parker, G. (2008) Experimental study of bedrock channel alluviation under varied sediment supply and hydraulic conditions. Water Resources Research, 44, W12446, doi: 10.1029/2007WR006581.

Chow, V.T. (1959) Open-channel hydraulics. McGraw Hill, New York.

Colebatch, G.T. (1941) Model tests on the Lawrence Canal roughness coefficients. Journal of the Institute of Civil engineers (Australia), 13(2), 27-32.

Comiti, F., Cadol, D. and Wohl, E. (2009) Flow regimes, bed morphology, and flow resistance in self-formed step-pool channels. Water Resources Research, 45, W04424, doi: 10.1029/2008WR007259.

Cox, R.G. (1973) Effective hydraulic roughness for channels having bed roughness different from bank roughness. A State-of-the-Art report. U.S. Army Engineer Waterways Experiment Station. Miscellaneous paper H-73-2. Vicksburg, Mississippi. 64 pp.

Czapiga, M. (2013) Systematic connectivity in single thread meandering alluvial rivers: statistical generalization of hydraulic geometry. MS Thesis. University of Illinois at Urbana-Champaign. 110 pp.

Einstein, H.A. (1934) Der Hydraulische oder Profil-Radius. Schweizerische Bauzeitung, Zurich. 103(8), 89-91.

Einstein, H.A. (1950) The bedload function for sediment transportation in open channel flows. Technical bulletin No. 1026, U.S.D.A. Soil Conservation Service, 1-71.

Ferguson, R.I., Hardy, R.J., and Hodge, R.A. (2019) Flow resistance and hydraulic geometry in bedrock rivers with multiple roughness length scales. Earth Surface Processes and Landforms. doi: 10.1002/esp.4673

Ferguson, R.I., Sharma, B.P., Hardy, R.J., Hodge, R.A., and Warburton, J. (2017a) Flow resistance and hydraulic geometry in contrasting reaches of a bedrock channel. Water Resources Research. 53, 2278-2293, doi: 10.1002/2016WR020233.

Ferguson, R.I., Sharma, B.P., Hodge, R.A., Hardy, R.J., and Warburton, J. (2017b) Bed

load tracer mobility in a mixed bedrock/alluvial channel. Journal of Geophysical Research: Earth Surface. 122, 807-822, doi: 10.1002/2016JF003946.

Fernández, R. (2012) Effect of width-to-depth ratio on the mean flow velocities for a Kinoshita meander bend. MS Thesis. University of Illinois at Urbana-Champaign. 75 pp.

Finnegan, N.J., Sklar, L.S. and Fuller, T.K. (2007) Interplay of sediment supply, river incision, and channel morphology revealed by the transient evolution of an experimental bedrock channel. Journal of Geophysical Research, 112, F03S11, doi: 10.1029/2006JF000569.

Garcia, M.H. (2008) Sedimentation Engineering—Processes, Measurements, Modeling, and Practice. ASCE Manuals and Reports on Engineering Practice No. 110. 1132 pp.

Gilbert, G.K. (1877) Report on the geology of the Henry Mountains. Department of the Interior, U.S. Geographical and Geological Survey of the Rocky Mountain Region. Washington, D.C. 214 pp.

Hodge, R., and Hoey, T.B. (2016a) A Froude-scaled model of a bedrock-alluvial channel reach: 1. Hydraulics. Journal of Geophysical Research: Earth Surface. 121, 1578-1596, doi: 10.1002/2015JF003706.Hodge, R., and Hoey, T.B. (2016b) A Froude-scaled model of a bedrock-alluvial channel reach: 2. Sediment cover. Journal of Geophysical Research: Earth Surface. 121, 1597-1618, doi: 10.1002/2015JF003709.

Hodge, R., Hoey, T., Maniatis, T., and Lepretre, E. (2016) Formation and erosion of sediment cover in an experimental bedrock-alluvial channel. Earth Surface Processes and Landforms. 41, 1409-1420, doi: 10.1002/esp.3924

Hodge, R., Hoey, T.B., and Sklar, L. (2011) Bed load transport in bedrock rivers: The role of sediment cover in grain entrainment, translation, and deposition. Journal of Geophysical Research. 116, F04028, doi: 10.1029/2011JF002032.

Horton, R.E. (1933) Separate roughness coefficients for channel bottoms and sides. Engineering News-Record, 3, 329-339.

Ikeda, S., Parker, G., and Sawai, K. (1981) Bend theory of river meanders. Part 1. Linear development. Journal of Fluid Mechanics. 112, 363-377.

Inoue, T., Izumi, N., Shimizu, Y. and Parker, G. (2014) Interaction among alluvial cover, bed roughness, and incision rate in purely bedrock and alluvial-bedrock channel. Journal of Geophysical Research: Earth Surface. 119, 2123-2146, doi: 10.1002/2014JF003133

Johanesson, H. and Parker, G. (1989) Linear theory of river meanders In Ikeda, S. and Parker, G. (Eds.) River Meadnering. Water Resources Monograph No. 12, American Geophysical Union, Washington D.C., 181-213.

Johnson, J.P.L. (2014) A surface roughness model for predicting alluvial cover and bed load transport rate in bedrock channels. Journal of Geophysical Research: Earth Surface. 119, 2147-2173, doi: 10.1002/2013JF003000.

Kamphuis, J.W. (1974) Determination of sand roughness for fixed beds. Journal of Hydraulic Research, 12(2), 193-203.

Keulegan, G.H. (1938) Laws of turbulent flow in open channels. Journal National Bureau of Standards, Research Paper 1151, 21, 707-741, Washington D.C.

Kikkawa, H. and Ishikawa, T. (1979) Resistance of flow over dunes and ripples. Proceedings Japan Society of Civil Engineering, 281, 53-63 (in Japanese).

Lotter, G.K. (1933) Considerations on hydraulic design of channels with different roughness of walls. Transactions of the All-Union Scientific Research Institute of Hydraulic Engineering. (9) 238-241. Leningrad.

Millar, R.G. (1999) Grain and form resistance in gravel-bed rivers. Journal of Hydraulic Research, 37(3), 303-312, doi: 10.1080/00221686.1999.9628249.

Nelson, P.A., Bolla Pittaluga, M., and Seminara, G. (2014) Finite amplitude bars in mixed bedrock-alluvial channels. Journal of Geophysical Research: Earth Surface. 119, 566-587, doi: 10.1002/2013JF002957.

Nelson, P.A., and Seminara, G. (2012) A theoretical framework for the morphodynamics of bedrock channels. Geophysical Research Letters, 39, L06408, doi: 10.1029/2011GL050806.

Nelson, J.M., and Smith, J.D. (1989) Flow in meandering channels with natural topography. In Ikeda, S. and Parker, G. (Eds.) River Meadnering. Water Resources Monograph No. 12, American Geophysical Union, Washington D.C., 69-102.

Nikuradse, J. (1933) Laws of flows in rough pipes (1950 translation of "Stromungsgesetze in rauhen Rohren." Forsch. Geb. Ingenieurwes., Ausg. Beill., 4, 361, 1933), National Advisory Committee of Aeronautics Tech Memo 1292, Washington D.C.

Otsu, N. (1979) A Threshold Selection Method from Gray-Level Histograms. IEEE Transactions on Systems, Man, and Cybernetics, 9(1), 62-66.

Parker, G. and Peterson, A.W. (1980) Bar resistance of gravel-bed streams. Journal of Hydraulic Engineering. Vol. 106(10), 1559-1575.

Pavlovskii, N.N. (1931) On a design formula for uniform flow in channels with nonhomogeneous walls. Transactions of the All-Union Scientific Research Institute of Hydraulic Engineering. (3) 157-164. Leningrad.

Rennie, C. D., Church, M., & Venditti, J. G. (2018). Rock Control of River Geometry: The

Fraser Canyons. Journal of Geophysical Research: Earth Surface. https://doi.org/10.1029/2017JF004458

Sklar, L., and Dietrich, W.E. (2004) A mechanistic model for river incision into bedrock by saltating bed load. Water Resources Research, 40, W06301, doi: 10.1029/2003WR002496.

Turowski, J. M., N. Hovius, A. Wilson, and M.-J. Horng (2008), Hydraulic geometry, river sediment and the definition of bedrock channels. Geomorphology, 99(1–4), 26–38, doi:10.1016/j.geomorph.2007.10.001.

Van Rijn, L.C. (1982) Equivalent roughness of alluvial bed. Journal of the Hydraulic Division, ASCE, 108(10). 1215-1218.

Vanoni, V.A., and Brooks, N.H. (1957) Laboratory studies of the roughness and suspended load of alluvial streams. Report No. E68, Sedimentation Laboratory, California Institute of technology, Pasadena, California.

Venditti, J.G., Rennie, C. D., Bomhof, J., Bradley, R. W., Little, M., and Chruch, M. (2014) Flow in bedrock canyons. Nature. 513: 534-537, doi:10.1038/nature13779.

Wright, S., and Parker, G. (2004) Flow resistance and suspended load in sand-bed rivers: Simplified stratification model density. Journal of Hydraulic Engineering, 130(8), 796-805.

Yasin, A.M. (1953) Mean roughness coefficient in open channels with different roughnesses of bed and side walls. PhD Thesis. Eidgenossischen Technischen Hochschule in Zurich. Switzerland. 94pp.

Yen, B.C., (2002) Open Channel Flow Resistance. Journal of Hydraulic Engineering, ASCE, 128(1), 20-39, doi: 10.1061/(ASCE)0733-9429(2002)128:1(20)

Yen, B.C. (1991) Hydraulic resistance in open channels. In B.C. Yen. (Ed.), Channnel flow resistance: Centennial of Manning's Formula (pp. 1-135).

Zhang, L., Parker, G., Stark, C. P., Inoue, T., Viparelli, E., Fu, X., and Izumi, N. (2016) Macro-roughness model of bedrock alluvial river morphodynamics. Earth Surface Dynamics, 3, 113–138, doi: 10.5194/esurf-3-113-2015.

List of tables

List of figures

Table 1 Experimental parameters, run ID and data source for the ten conditions.

Data Source	Run ID	Condition	Discharge Q (Ls^{-1})	Mean Depth H (m)	Mean Water-Surface Slope S x 10^3 (-)	Reach-averaged Velocity U (ms^{-1})	Froude Fr (-)	Reynolds Re (-)
Fernandez (2012)	F1	Flat-smooth	25	0.25	0.051	0.17	0.11	22,282
	F2	Flat-smooth	25	0.15	0.396	0.28	0.23	27,233
	F3	Flat-smooth	8	0.05	0.732	0.27	0.38	11,204
Abad and Garcia (2009)	F4	Flat-smooth	50	0.25	0.450	0.33	0.21	44,563
Czapiga (2013)	A1	Alluvial	12.3	0.078	2.800	0.26	0.30	15,951
	A2	Alluvial	12.3	0.071	3.100	0.29	0.35	16,252
	A3	Alluvial	3	0.043	3.700	0.12	0.18	4,287
This study	B1	Bedrock	12.5	0.110	0.770	0.19	0.18	14,945
	BA1	Bedrock-alluvial	12.5	0.110	0.631	0.19	0.18	14,945
	BA2	Bedrock-alluvial	12.5	0.114	1.320	0.18	0.17	14,808

Table 2 Dimensionless friction coefficients for the Kinoshita flume with flat bed.

Run ID	(C_f, f, C_z)		
	Total [a]	Wall [b]	Meandering [c]
F1	(0.0025, 0.0196, 20.2)	(0.0023, 0.0184, 20.8)	(0.0001, 0.0012, 82.7)
F2	(0.0050, 0.0403, 14.1)	(0.0022, 0.0177, 21.3)	(0.0028, 0.0226, 18.8)
F3	(0.0043, 0.0346, 15.2)	(0.0027, 0.0214, 19.3)	(0.0016, 0.0132, 24.6)
F4	(0.0054, 0.0433, 13.6)	(0.0020, 0.0160, 22.4)	(0.0034, 0.0273, 17.1)

[a] Computed with Eqs. 8 and 6.
[b] Computed with Eq. 16
[c] Computed with Eq. 19

Table 3 Dimensionless friction coefficients for fully alluvial, bedrock, and mixed bedrock-alluvial beds.

Run ID	(C_f, f, C_z)				
	Total	Wall correction		Shear partition	
		Wall	Bed	Skin[a]	Form
A1	(0.0246, 0.1968, 6.4)	(0.0039, 0.0312, 16.0)	(0.0300, 0.2400, 5.8)	(0.0101, 0.0808, 10.0)	(0.0199, 0.1592, 7.1)
A2	(0.0209, 0.1672, 6.9)	(0.0038, 0.0304, 16.2)	(0.0250, 0.2000, 6.3)	(0.0098, 0.0784, 10.1)	(0.0152, 0.1216, 8.1)
A3	(0.1010, 0.8080, 3.1)	(0.0074, 0.0592, 11.6)	(0.1144, 0.9152, 3.0)	(0.0204, 0.1632, 7.0)	(0.0940, 0.7520, 3.3)
B1	(0.0169, 0.1352, 7.7)	(0.0037, 0.0296, 16.4)	(0.0218, 0.1744, 6.8)	(0.0128, 0.1024, 8.8)	(0.0090, 0.0720, 10.5)
BA1	(0.0139, 0.1112, 8.5)	(0.0035, 0.0280, 16.9)	(0.0177, 0.1416, 7.5)	(- , - , -)	(- , - , -)
BA2	(0.0319, 0.2552, 5.6)	(0.0042, 0.0336, 15.4)	(0.0424, 0.3392, 4.9)	(- , - , -)	(- , - , -)

[a] $k_s = 2.5\ D_{90}$; for A1-A3 $D_{90} = 1.9$ mm and for B1 $D_{90} = 7.5$ mm

Table 4 Dimensionless friction coefficients for the mixed bedrock-alluvial experiments.

Run ID p_c		(C_f, f, C_z) Johnson			Inoue
		Alluvial [a]	Bedrock [b]	Combined [c]	Composite k_s [d]
BA1	Skin	(0.008, 0.062, 11.3)	(0.012, 0.097, 9.1)	(0.011, 0.090, 9.5)	(0.011, 0.091, 9.4)
p_c = 0.21	Form	(0.010, 0.079, 10.1)	(0.006, 0.044, 13.5)	(0.006, 0.051, 12.5)	(0.006, 0.050, 12.7)
BA2	Skin	(0.010, 0.080, 10.0)	(0.016, 0.130, 7.8)	(0.011, 0.091, 9.4)	(0.012, 0.095, 9.2)
p_c = 0.78	Form	(0.032, 0.258, 5.6)	(0.026, 0.208, 6.2)	(0.031, 0.247, 5.7)	(0.031, 0.244, 5.7)

[a] Calculated assuming fully alluvial conditions, i.e. D_{90} = 1.9 mm and $k_s = 2.5D_{90}$.
[b] Calculated assuming bare bedrock conditions; i.e. D_{90} = 7.5 mm and $k_s = 2.5D_{90}$.
[c] Calculated with Eq. 14; f_a and f_b from previous two columns respectively.
[d] Calculated with unique composite roughness as in Eq. 13.

Table 5 Equivalent roughness heights.

Run ID	(Total, Wall, Bed, Skin, Form)		
	R_H	C_f	k_s
	(cm)	(-)	(mm)
F1	(13.6, - , -, 13.6, 13.6)	(0.0024, - , -, 0.0023, 0.0001)	(0.38, - , -, 0.29, 0.00)
F2	(10.0, - , - , 10.0, 10.0)	(0.0050, - , -, 0.0022, 0.0028)	(3.41, - , -, 0.18, 0.49)
F3	(4.3, - , - , 4.3, 4.3)	(0.0043, - , -, 0.0027, 0.0016)	(0.92, - , -, 0.17, 0.02)
F4	(13.6, - , - , 13.6, 13.6)	(0.0054, - , -, 0.0020, 0.0034)	(5.71, - , -, 0.16, 1.35)
A1	(6.2, 1.0, 7.5, 2.5, 5.0)	(0.025, 0.004, 0.030, 0.010, 0.020)	(49.9, 0.2, 77.8, 4.7, 30.1)
A2	(5.7, 1.0, 6.9, 2.7, 4.2)	(0.021, 0.004, 0.025, 0.010, 0.015)	(37.2, 0.1, 56.4, 4.7, 16.5)
A3	(3.8, 0.3, 4.3, 0.8, 3.5)	(0.101, 0.007, 0.114, 0.020, 0.094)	(114, 0.3, 139, 4.7, 101)
B1	(8.0, 1.7, 10.4, 6.2, 4.2)	(0.017, 0.004, 0.022, 0.013, 0.009)	(37.9, 0.2, 70.9, 18.7, 5.8)
BA1	(8.0, 2 .0, 10.3, 6.6, 3.6)	(0.014, 0.004 , 0.018, 0.011, 0.006)	(27.3, 0.2, 51.7, 15.7, 2.2)
BA2	(8.3, 1.1, 11.0, 3.1, 7.9)	(0.032, 0.004 , 0.042, 0.012, 0.031)	(91.3, 0.2, 165, 7.9, 83.0)

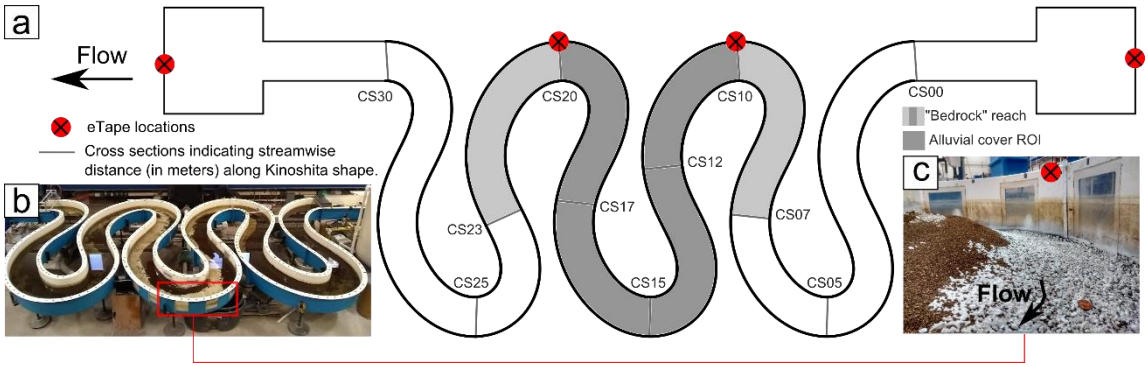

Figure 1. (a) Kinoshita flume sketch with eTape locations and a few cross sections indicating streamwise distance along the Kinoshita shape; (b) Kinoshita flume side view image with rectangle indicating approximate area shown in (c); (c) Partially alluviated bed inside the Kinoshita flume, eTape is shown in the back. Shaded areas indicate bedrock reach in experiments B, BA1 and BA2. Darker shade indicates the region of interest (ROI) used to measure alluvial cover.

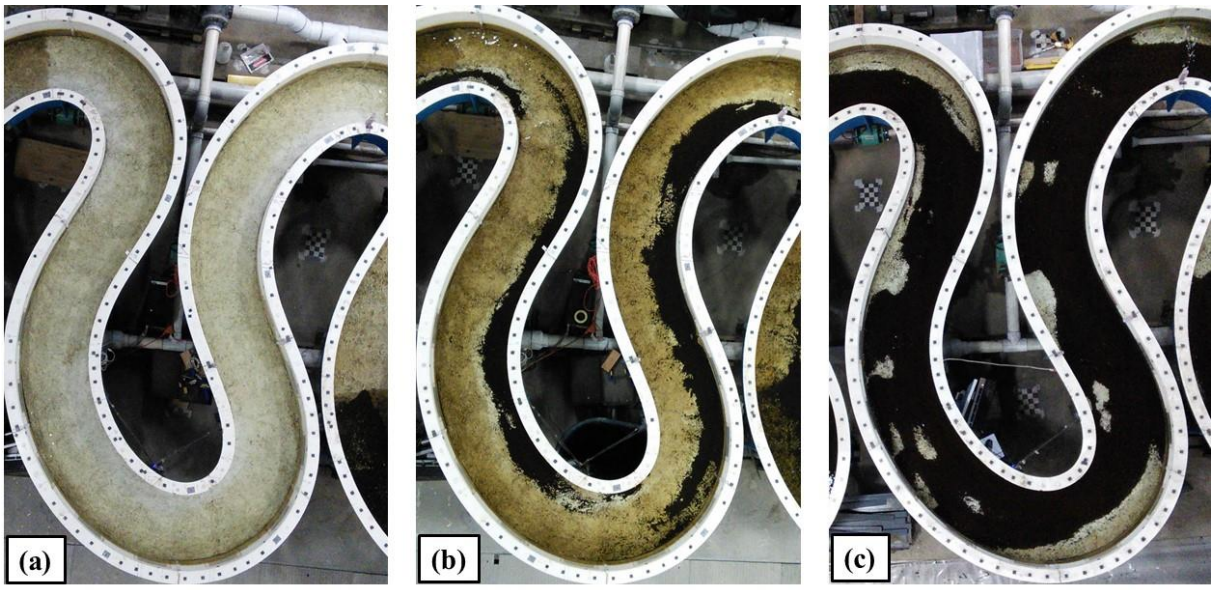

Figure 2. Images of the middle bend of the Kinoshita flume with (a) no areal cover (bare bedrock); (b) 21% areal cover and (c) 78% areal cover.

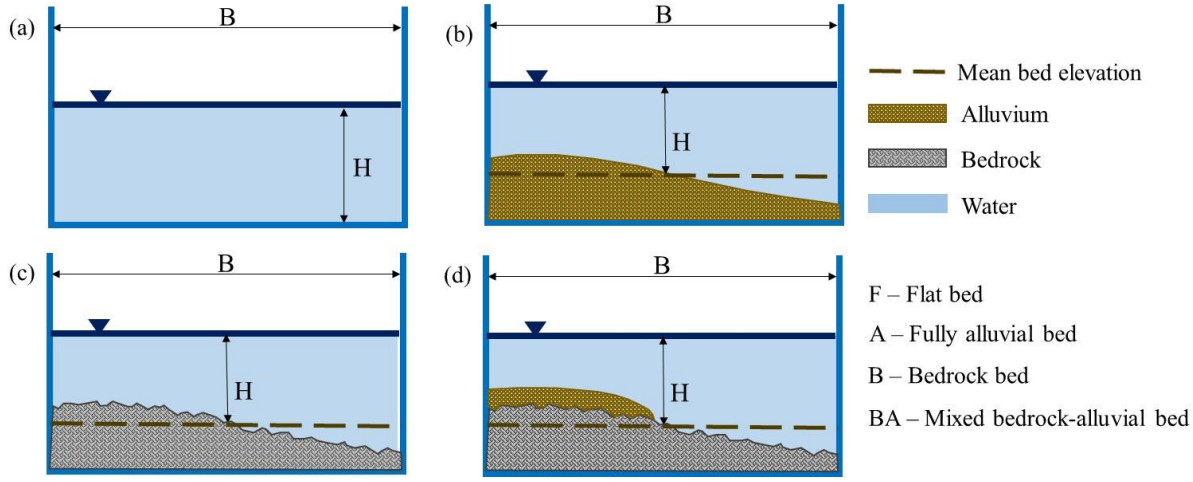

Figure 3. Experimental conditions used: (a) Flat, smooth bed and no sediment - F; (b) Fully alluvial bed - A; (c) Bedrock bed - B; (d) Mixed bedrock-alluvial bed - BA.

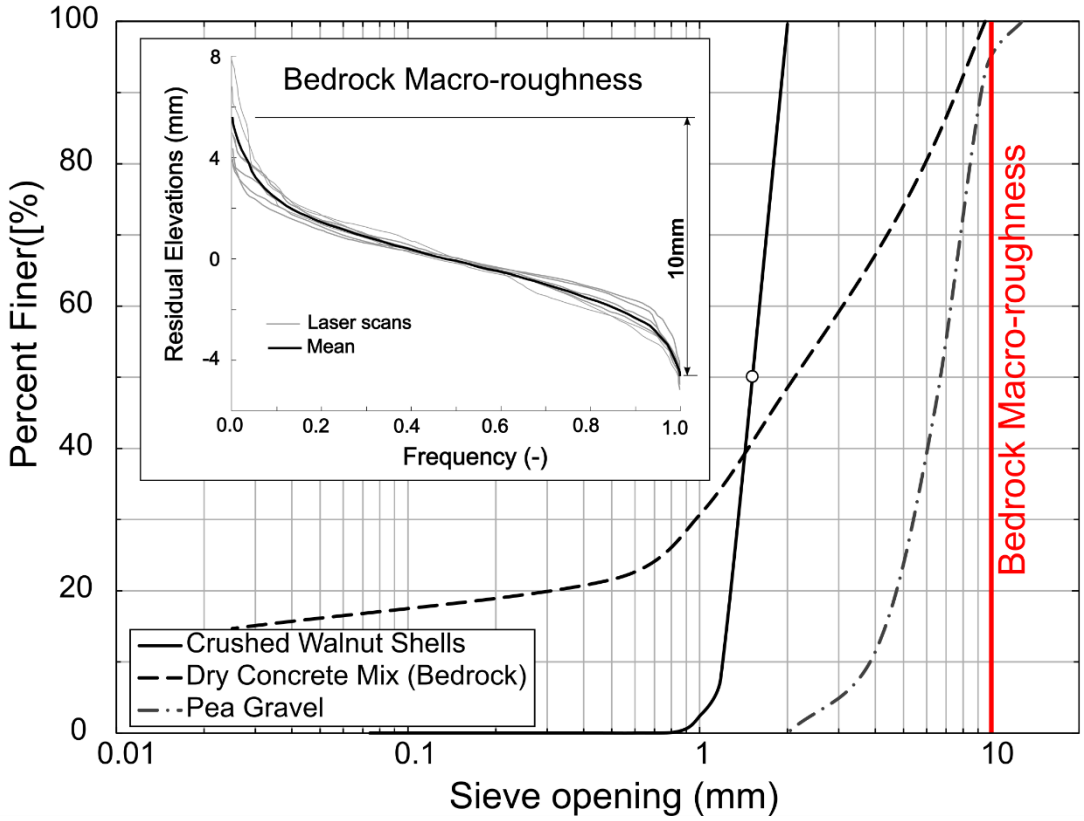

Figure 4. Grain size distributions for the crushed walnut shells, dry concrete mix used to build the bedrock, and the pea gravel underlying the bedrock basement. Insert shows residual elevations of as-built bedrock bed, measured with laser scans at different cross sections inside the Kinoshita flume. Mean macro-roughness (~10mm) is also indicated in the main plot.

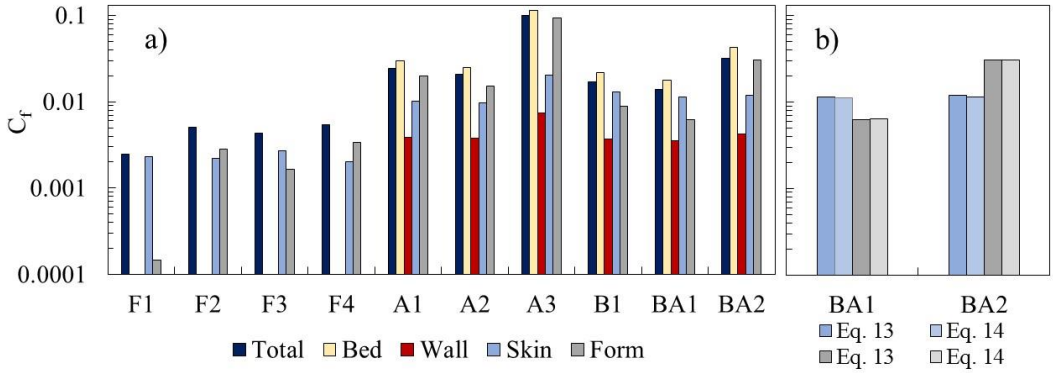

Figure 5 a) Dimensionless friction coefficient values for all runs. b) Skin and form friction coefficients obtained with the approaches of Inoue et al. (2014) (Eq. 13), and Johnson (2014) (Eq. 14).

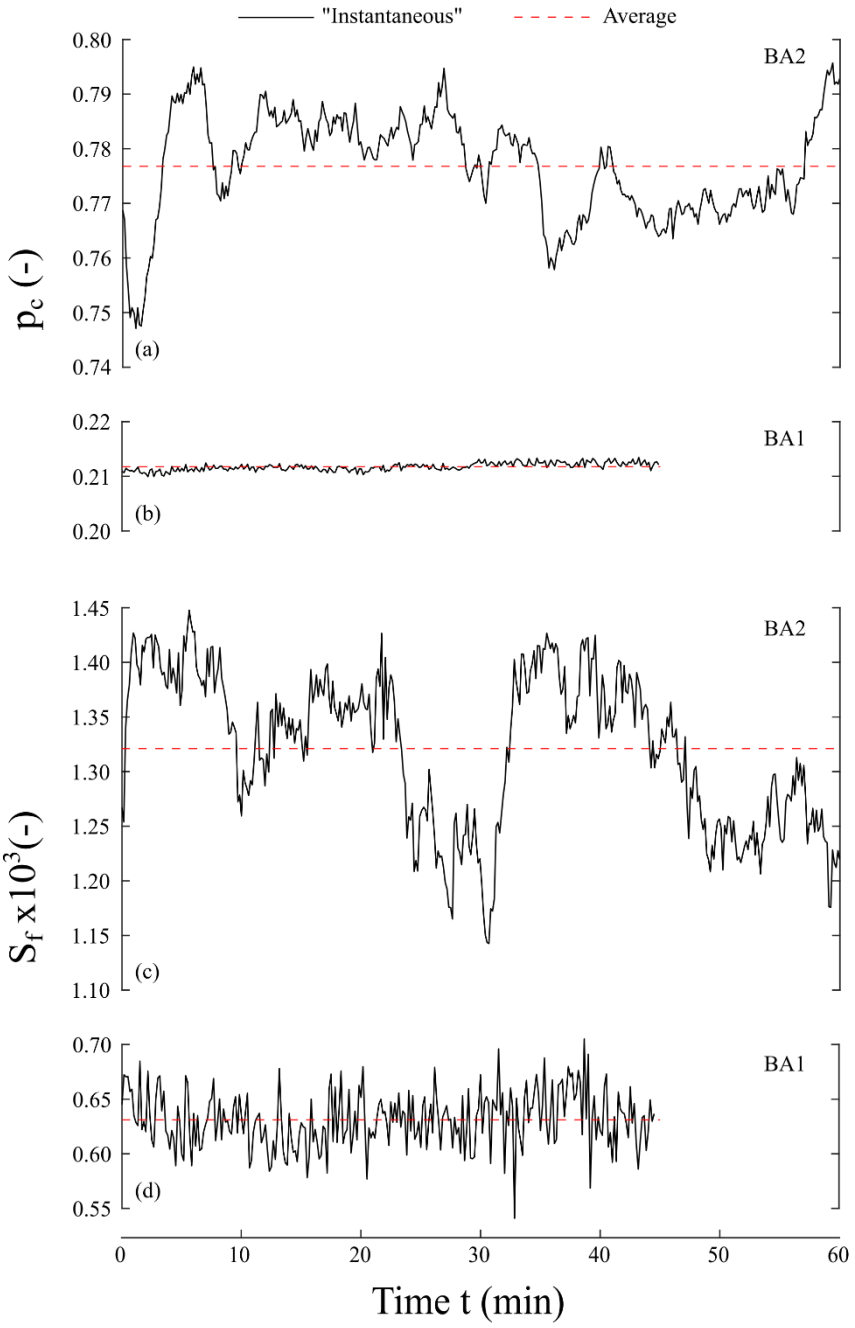

Figure 6 Temporal series of alluvial cover for runs (a) BA2 and (b) BA1; and temporal series of water surface slope for runs (c) BA2 and (d) BA1.

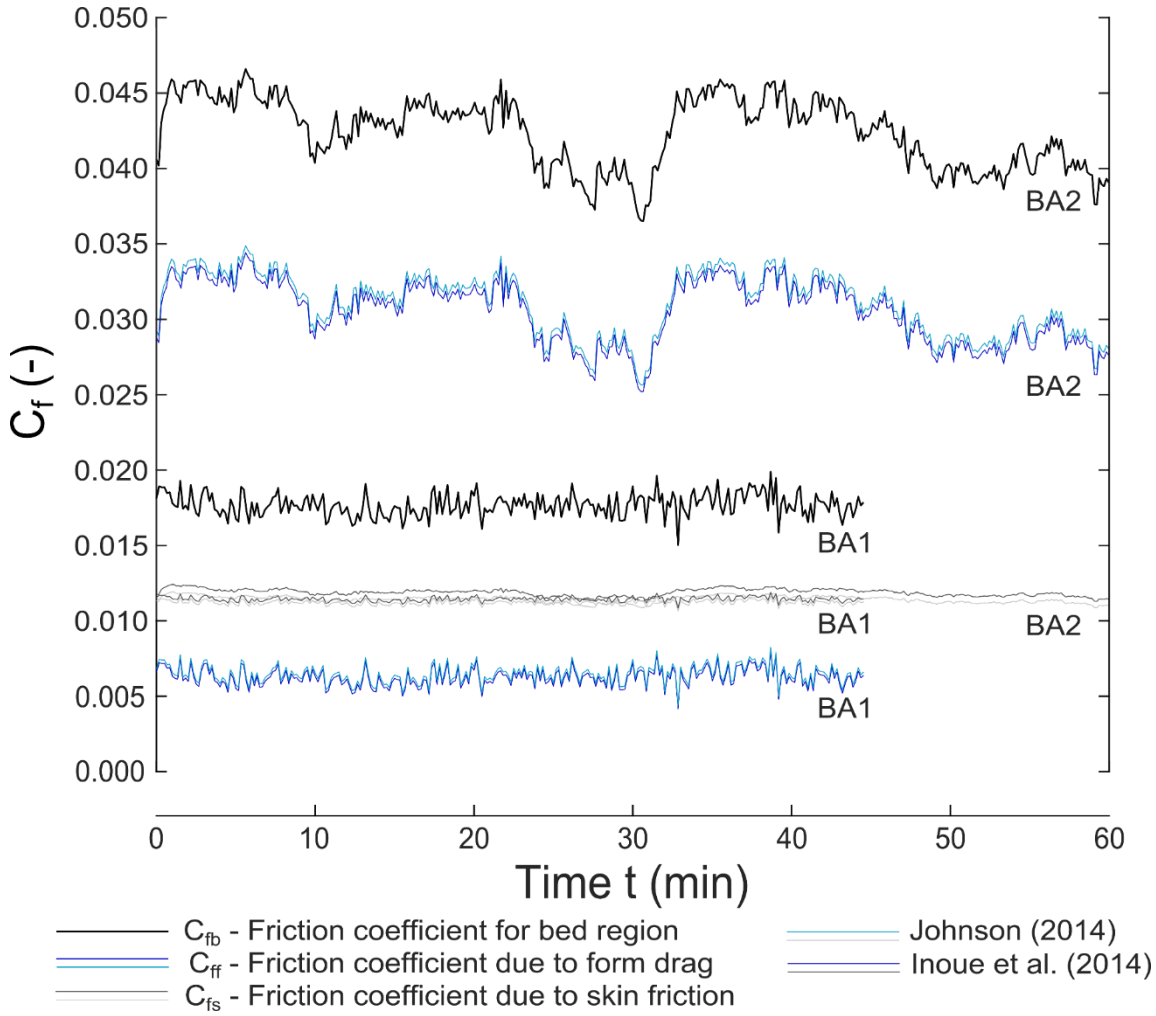

Figure 7. Temporal series of dimensionless friction coefficients for runs BA1 and BA2.

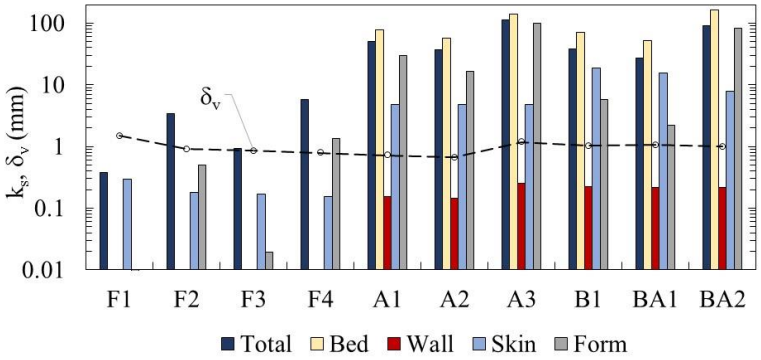

Figure 8. Equivalent roughness heights for all runs. The thickness of the viscous sublayer is shown for reference. Note that the walls of the Kinoshita flume are hydraulically smooth ($k_s < \delta_v$).

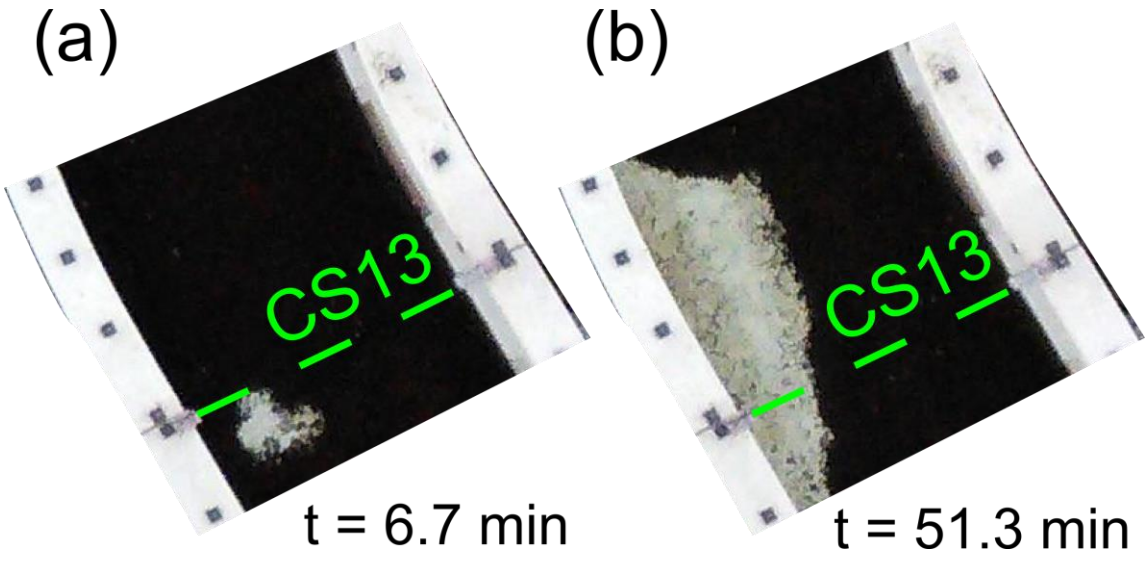

Figure 9. Local variation in instantaneous alluvial cover during run BA2. (a) p_c = 0.97 and (b) p_c = 0.70. Flow from bottom. Window area: W = 0.6 m L ~ 0.8 m.